IRIS AperTO

UNIVERSITÀ DEGLI STUDI DI TORINO

AperTO - Archivio Istituzionale Open Access dell'Università di Torino

Parameterization of shortwave, longwave and net radiation fluxes over the Hells Gate ice shelf (Antarctica)

This is the author's manuscript

Original Citation:

Availability:

This version is available http://hdl.handle.net/2318/17787 since

Publisher:

SIF - Editrice Compositori

Terms of use:

Open Access

Anyone can freely access the full text of works made available as "Open Access". Works made available under a Creative Commons license can be used according to the terms and conditions of said license. Use of all other works requires consent of the right holder (author or publisher) if not exempted from copyright protection by the applicable law.

(Article begins on next page)

05 May 2023

Conference Proceedings Vol. 80
"Italian Research on Antarctic Atmosphere"
M. Colacino, (Ed.)
SIF, Bologna, 2002

Parameterization of shortwave, longwave and net radiation fluxes over the Hells Gate ice shelf (Antarctica)

S. Ferrarese[1], M. Qian[1], D. Bertoni[1], C. Cassardo[1], R. Forza[1], T. Georgiadis[2], A. Longhetto[1], M. Nardino[2] and M. Pangia[3]

[1] Department of General Physics, University of Turin, Italy
[2]ISAC/CNR Bologna, Via P. Gobetti 101 - 40129 Bologna, Italy
[3] ISAC/CNR Roma, Area di Ricerca di Roma Tor Vergata
Via del Fosso del Cavaliere, 100 - 00133 Roma, Italy

Abstract

During the southern summer of 1997-1998, the XIII Antartic scientific expedition organized by the PNRA took place at the Italian base of Terra Nova Bay. In this expedition, the team of IFA (CNR, now ISAC Roma) measured global shortwave radiation fluxes, temperature, humidity and pressure over the Hells Gate ice shelf. In the same period and at a very nearby site, the team of ISAO (CNR, now ISAC Bologna) measured the fluxes of incident and reflected shortwave radiations, upward and downwarlongwave radiations, and the albedo. In this work, the different components of the net radiation (incoming and outcoming shortwave and longwave) are calculated using the data collected by IFA with some parameterizations found in the literature. The results are compared with the observations performed by ISAO with the aim to verify the parameterizations, important for assessing the land surface process in Antarctica. The first results show periods and situations of good agreement and other situations in which the departure of calculated data from observations is not negligible. A discussion of these results is presented.

1 Introduction

The energy budget at the interface between bare soil and atmosphere can be expressed as:

$$R_n = L_e E + H + G \tag{1}$$

where R_n is the net radiation, $L_e E$ is the latent heat flux, H is the sensible heat flux, and G is the heat flux entering into the surface through conduction. The net radiation can be broken down into several components:

$$R_n = S_n + L_n = S_{in} - S_{out} + L_{in} - L_{out} \tag{2}$$

where S_n is the shortwave net radiation, L_n the longwave net radiation, S_{in} the incoming shortwave radiation, S_{out} the outcoming shortwave radiation, L_{in} the incoming longwave radiation and L_{out} the outcoming longwave radiation.

Whenever possible, the net radiation flux should be measured as well and, at present, fairly reliable instruments are available for this purpose. However, in absence of direct measurements, net radiation can be estimated from its components. When the observation of these measurements are not available, the components can be obtained by theoretical methods or simple empirical formulae (parameterization).

In some previuos work [1, 2] the attention has been focused on the evaluation of energy balance, while the aim of this work is to test some parameterizations of short and longwave radiation present in the literature. Some intercomparisons between measured and parameterized data will be presented and checked.

2 Experimental layout

Some measured data were collected by ISAO (CNR Bologna) in the site located in the position identified by the latitude-longitude coordinates: 74° 51' 3.7" S, 163°, 47', 2.8" E. The instruments were: a pyrradiometer Schenk model 8111 (range: 0.3-60μm), an albedometer Schenk model 8104 (range: 0.3-3μm), a pyrgeometer Eppley model PYR (range: $> 3\mu$m), and a pyrgeometer Everest model 4000.4GL. They allow to measure:

- the incident and reflected shortwave radiations and albedo (respectively S_{inM}, S_{outM}, α_M);
- the downward and upward longwave radiations (respectively L_{inM}, L_{outM}).

In the site located in the position: 74° 52' 20.2" S, 163° 49' 6.4" E, the team of IFA (CNR, Roma) collected other data:

- the global shortwave radiation (S_{inR}) by the Solarimeter Sitep (range: 0.4-1.1μm);

- the temperature of air and ice surface (T_a, T_s) by the Thermometers Sitep (range: -30 - 70° C) at 5m and surface;

- the humidity (r_h) by the Sitep hygrometer (range: 0-100%) at 5m;

- the pressure (p) by the Sitep barometer (range: 800 - 1100 hPa).

The data measured by IFA team have been used to calculate the components of radiation (S_{in}, S_{out}, L_{in} and L_{out}).

Two periods of this campaign, in which all instruments where operational have been selected. The first one ranged from 12^{th} of January 1998 to 26^{th} of January 1998 and the second one from 3^{rd} of February 1998 to 18^{th} of February 1998. They will hereafter be referenced as first and second period respectively.

3 Results

3.1 Incoming shortwave radiation

The measurements ranges of the two instruments, *i.e.* the Albedometer Schenk (0.3-3.0μm) and the Solarimeter Sitep (0.4-1.1μm), are different and have two non overlapping sub-ranges (0.3-0.4μm and 1.1-3.0μm). The incoming shortwave radiation has been parameterized, taking into account the missing range in the following way:

1) the solar elevation γ [3] has been computed using the input data: time, longitude and latitude;

2) the relative optical air mass (m) [3] has been calculated as:

$$m = \frac{1 - \frac{z}{8000}}{sin(\gamma)} \qquad \text{if } \gamma > 10^0 \tag{3}$$

$$m = \frac{1 - \frac{z}{8000}}{sin(\gamma) + 0.15(\gamma + 3.885)^{-1.253}} \qquad \text{if } \gamma < 10^0 \tag{4}$$

where z is the altitude of the site;

3) the incoming shortwave radiation (S_{in}) has been computed as:

$$S_{in} = S_{inR} + \frac{0.025 \cdot S_{inR}}{0.1 * m} \quad \text{if January} \tag{5}$$

$$S_{in} = S_{inR} + \frac{0.05 \cdot S_{inR}}{0.1 * m} \quad \text{if February} \tag{6}$$

where the coefficient 0.025 and 0.05 depend on the solar elevation.

The results are displayed in figs. 1(a) and 1(b). The fig. 1(a) is relative to the first period (from 12^{th} to 26^{th} of January) while the fig. 1(b) is relative to the second period (from 3^{rd} to 18^{th} of February). In abscissa the julian day is shown. The star points represent the measured data (S_{inM}), the dashed line the measures collected by the solarimeter Sitep (S_{inR}), the solid line the parameterized results (S_{in}) and the dashdot line is the theoretical incoming radiation under clean sky (S_{inT}), which is calculated according to [3] and [4]. It is noticeable that there is a good agreement between the measured and the parameterized data in both periods, and during clear and cloudy sky days.

In order to get a quantitive index, quantities named DIFF and BIAS have been calculated according to the relations:

$$DIFF = \frac{\sum_{i=1}^{N}[x_{par}(i) - x_{obs}(i)]}{N} \tag{7}$$

$$BIAS = \frac{\sum_{i=1}^{N}|x_{par}(i) - x_{obs}(i)|}{N} \tag{8}$$

where x_{par} is the parameterized value, x_{obs} the measured one and N the total number of data. In table 1, the values of DIFF and BIAS for the comparison between S_{in} and S_{inM} are reported. Considering that the instrumental precision of the Sitep solarimeter is $\pm 15 \mathrm{Wm}^{-2}$, it is clear that BIAS has the same order of the precision.

Table 1: Statistics about incoming shortwave radiation fluxes

Incoming shortwave radiation flux	DIFF	BIAS
S_{in} - S_{inM} $\left(\mathrm{Wm}^{-2}\right)$	-4	24

The theoretical incoming radiation under clean sky has been used to evaluate the cloudiness. In fact, as it can be seen by looking figs. 1(a) and 1(b), the 15^{th}, 35^{th}, and 45^{th} julian days can be considered as clear sky days, because S_{inT} is almost equal to S_{inM}, while, during the other days, the presence of cloudiness is evident and cannot be neglected.

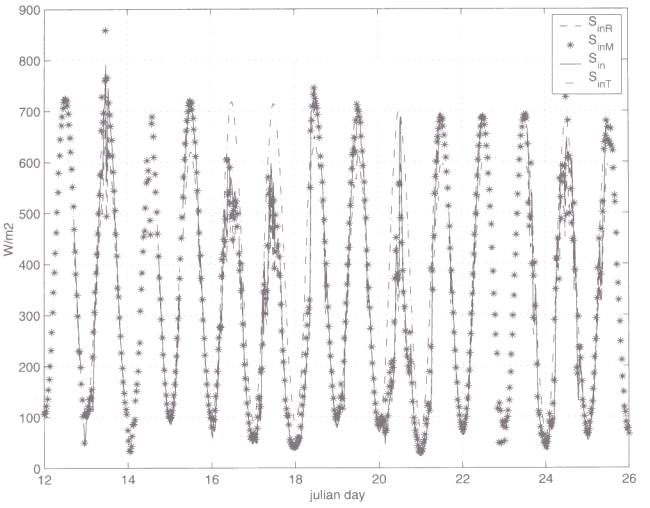

(a) Incoming shortwave radiation, January 1998.

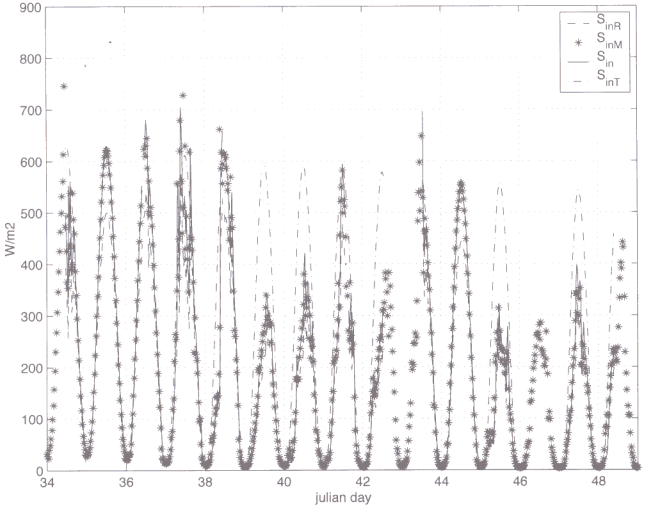

(b) Incoming shortwave radiation, February 1998.

Figure 1: In the abscissa the julian days are reported. The star points refer to S_{inM}, the dashed line to S_{inR}, the solid line to S_{in} and the dashdot line to S_{inT}; all values are expressed in Wm^{-2}.

3.2 Outcoming shortwave radiation

The relation between incoming and outcoming shortwave is:

$$S_{out} = \alpha \cdot S_{in} \tag{9}$$

where α is the albedo of the surface.

As the antarctic soil is covered by snow, to reconstruct the albedo trend, two relations have been used:

1) Iqbal [5]:

$$\alpha 1 = \alpha' + (1 - \alpha') \exp\left[-0.1\gamma - \frac{1 - \alpha'}{2}\right] \tag{10}$$

where α' is the albedo at the maximum solar elevation and γ is the solar altitude. In these simulations, the values: α'=0.8 in January and α'=0.62 in February have been imposed;

2) Loth and Graf [6], Verseghy [7]:

$$\alpha 2(t) = \alpha_0(t) + \alpha_0^3(t)\,[1 - a_0(t)]\,F \tag{11}$$

$$\alpha_0(t) = \alpha + [\alpha_0(t - \Delta t) - a] \exp\left(-0.01 \frac{\Delta t}{3600}\right) \tag{12}$$

$$F = N^2 + \exp\left(sin^2\varphi\right) - 1.3N^2 \exp\left(cos^2\varphi\right) \tag{13}$$

where a=0.5, N is the amount of clouds and φ the minimum between the actual sun elevation and $\frac{\pi}{3}$.

In the simulations, the values: $\alpha = 0.6$, $\alpha_0(0) = 0.72$ and $\alpha_0(t) = 0.72$ (in case of snow) have been used. The main difference between the two parameterizations of albedo is that in the second parameterization the amount of clouds and the presence of snow are considered.

Then, the two values:

$$S_{out1} = \alpha 1 \cdot S_{in} \tag{14}$$

$$S_{out1} = \alpha 2 \cdot S_{in} \tag{15}$$

have been calculated and shown in figs. 2(a) and 2(b).

As in the previous figures, the star points represent the measured data (S_{outM}), while S_{out1} is the dashed line and S_{out2} is the solid line, and in the abscissa there are the julian days. The agreement between the measured and parameterized data is good for both formulations, and BIAS (table 2) is similar to the one of incoming radiation. During the first period, eq. 10 generally behaves better (table 2). But, during the last snowy days, (from 45^{th} to 47^{th} julian days) the eqs. 11 - 13 show a better behaviour.

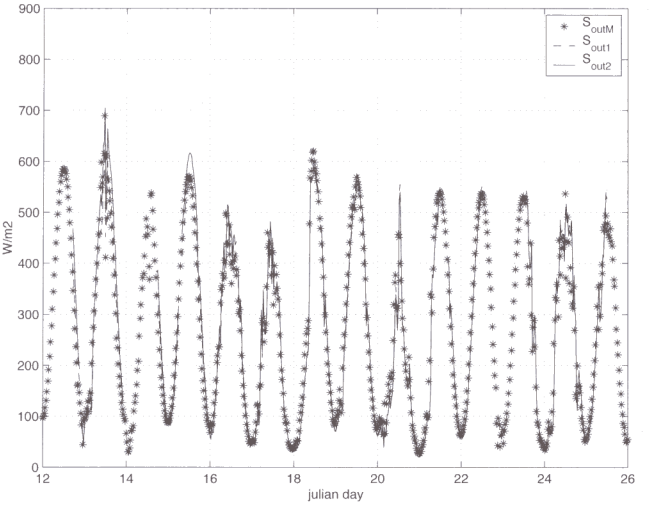

(a) Outcoming shortwave radiation, January 1998.

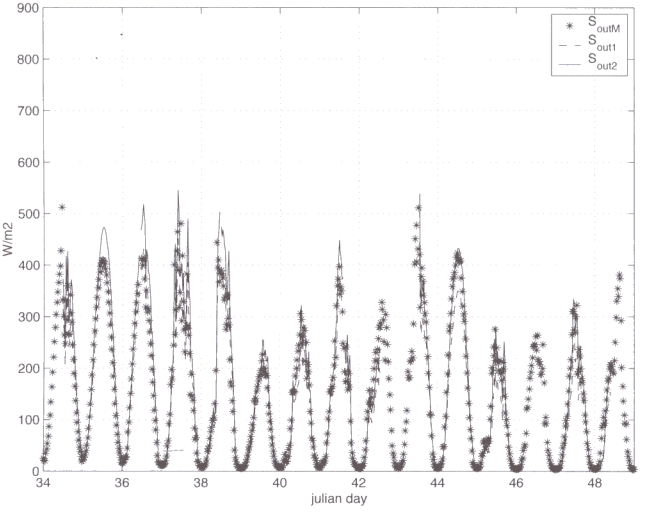

(b) Outcoming shortwave radiation, February 1998.

Figure 2: In the abscissa the julian days are reported. The star points refer to S_{outM}, the dashed line to S_{out1} and the solid line to S_{out2}; all values are expressed in Wm^{-2}.

Table 2: Statistics about outcoming shortwave radiation fluxes

Outcoming shortwave radiation flux	DIFF	BIAS
S_{out1} - S_{outM} $\left(\mathrm{Wm}^{-2}\right)$	-8	28
S_{out2} - S_{outM} $\left(\mathrm{Wm}^{-2}\right)$	10	29

3.3 Incoming longwave radiation

The incoming longwave radiation is expressed by the product of two terms: L_{in-c}, the incoming longwave radiation under clean sky, and the cloudiness index:

$$L_{in} = L_{in-c} \cdot cloudiness \tag{16}$$

L_{in-c} has been computed using a parameterization based on the law of gray bodies:

$$L_{in-c} = e_{ac}\sigma T_a^4 \tag{17}$$

where e_{ac} is the equivalent of the emissivity of atmosphere, σ the Stefan-Boltzmann constant (equal to $5.67 \cdot 10^{-8}\mathrm{WK}^{-4}$) and T_a the air temperature. For the parameterization of e_{ac}, three schemes have been used:

$$e_{ac} = 0.95\left[1 - \exp\left(-e_a^{T_a/2016}\right)\right] \qquad \text{Satterlund [8]} \tag{18}$$

$$e_{ac} = 0.6\left(e_a^{0.08}\right) \qquad \text{Stanley } et\ al. \text{ [9]} \tag{19}$$

$$e_{ac} = 0.85 \cdot 10^{-5} T_a^2 \qquad \text{Swinbank [10]} \tag{20}$$

The numerical coefficients have been slightly modified with respect to the original formulations to take into account the peculiar (snowy) surface in Antarcica. In fact, in the eq. 18 the original factor was 1.08, in eq. 19 it was 0.67, and in eq. 20 it was 0.92. For the parameterization of e_a, the usual equation:

$$e_a = \frac{r_h}{100} \cdot E \tag{21}$$

$$E = 6.112 \exp\left(17.67 \frac{T_a - 273.15}{T_a - 29.65}\right) \qquad \text{Garratt [11]} \tag{22}$$

has been used. In the previous relation, r_h is the relative humidity and E is the water vapour pressure at the saturation. The main difference between the three parameterizations given by eqs. 18 to 20 is that the first two formulae contain an explicit dependence from temperature and humidity, while the third one is depending only from temperature.

Finally, the parameterizations used to evaluate the cloudiness are:

$$cloudiness = 1.8 - 0.8\frac{S_{in}}{S_{inT}} \quad \text{for parameterization (18) and (19)} \quad (23)$$

$$cloudiness = 1.93 - 0.93\frac{S_{in}}{S_{inT}} \quad \text{for parameterization (20)} \quad (24)$$

adapted by Brutsaert [12] for antarctic conditions. These calculations can obviously be done only when $S_{inT} \neq 0$, then during daytime. For this reason, the nocturnal hours haven't been considered in this work; as the study refers to the Summer season, the number of radiationless nights was limited to few days in February.

The values of cloudiness obtained by eqs. 23 and 24 have been smoothed using a running average of fifth order. In the following L_{in1}, L_{in2} and L_{in3} are defined as the incoming longwave radiations eq. 16 where e_{ae} has been computed using eqs. 18, 19 and 20 respectively.

The result of the parameterizations given by eq. 18 [8] is reported in figs. 3(a) and 3(b). As usual, the star points represent the measured data. In this case, the dashed line is the incoming longwave radiation under clean sky conditions and the solid line is the incoming longwave radiation with cloudiness. It is clear from these graphics that the cloudiness term is important, even if the agreement between measured and parameterized data is not perfect.

In figs. 4(a) and 4(b), the parameterization of incoming longwave radiation given by eq. 19 is represented. It can be observed that this equation has a behaviour similar to the 18.

The parameterization of incoming longwave radiation given by 20 is shown in figs. 5(a) and 5(b). In this case, the differences between observations and parameterizations are larger than in the previous two cases.

In table 3 the values of DIFF and BIAS for the comparison between L_{in1}, L_{in2}, L_{in3} and L_{inM} are reported. The numerical values confirm the qualitative conclusions inferred by graphics analysis above. The values of bias are smaller than the ones relative to the short wave radiation.

3.4 Outcoming longwave radiation

The outcoming longwave radiation (L_{out}) is usually obtained using the law of gray body:

$$L_{out} = \varepsilon\sigma T_s^4 \quad (25)$$

where ε is the emissivity, σ is the Stefan-Boltzmann constant and T_s is the surface temperature. The value $\varepsilon = 0.97$ reported in the literature [12] for

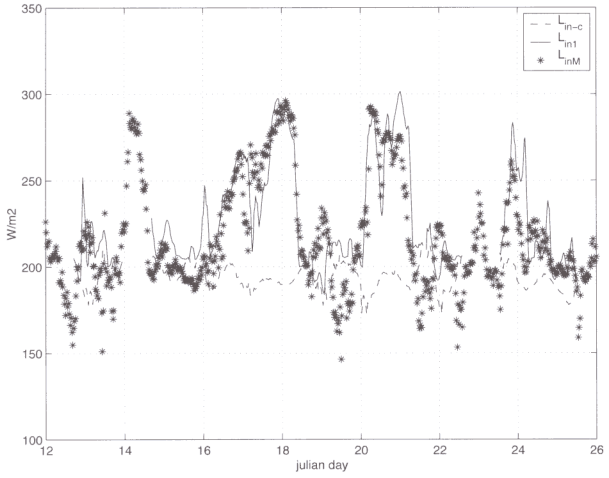

(a) Incoming longwave radiation from Satterlund (1979), January 1998.

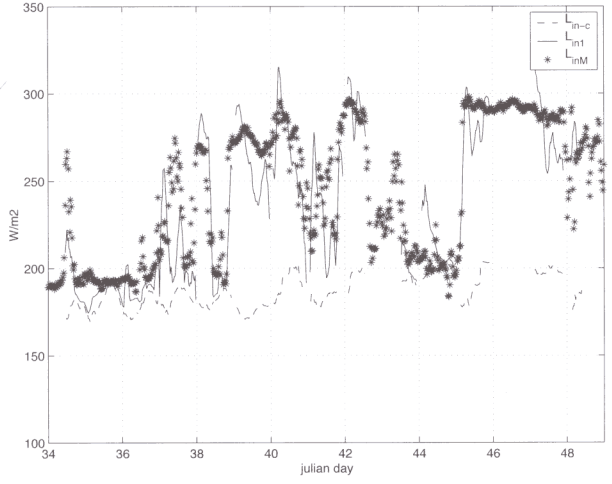

(b) Incoming longwave radiation from Satterlund (1979), February 1998.

Figure 3: In the abscissa the julian days are reported. The star points refer to L_{inM}, the dashed line to L_{in-c} and the solid line to L_{in1}; all values are expressed in Wm^{-2}.

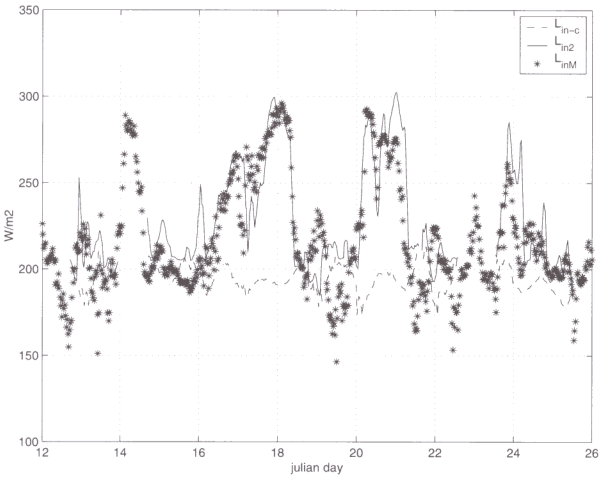

(a) Incoming longwave radiation from Stanley *et al.* [9], January 1998.

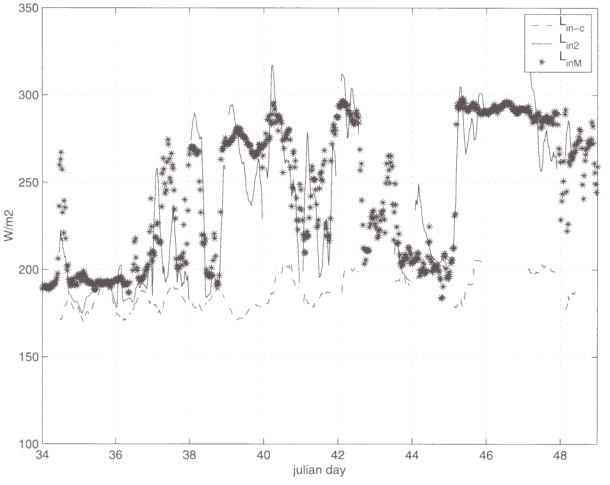

(b) Incoming longwave radiation from Stanley *et al.* [9], February 1998.

Figure 4: In the abscissa the julian days are reported. The star points refer to L_{inM}, the dashed line to L_{in-c} and the solid line to L_{in2}; all values are expressed in Wm^{-2}.

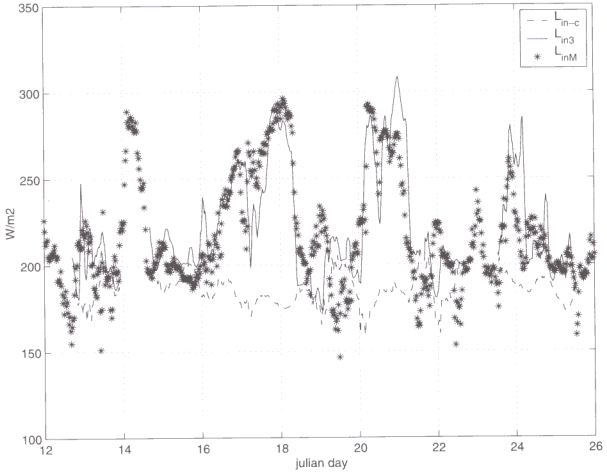

(a) Incoming longwave radiation from Swinbank [10], January 1998.

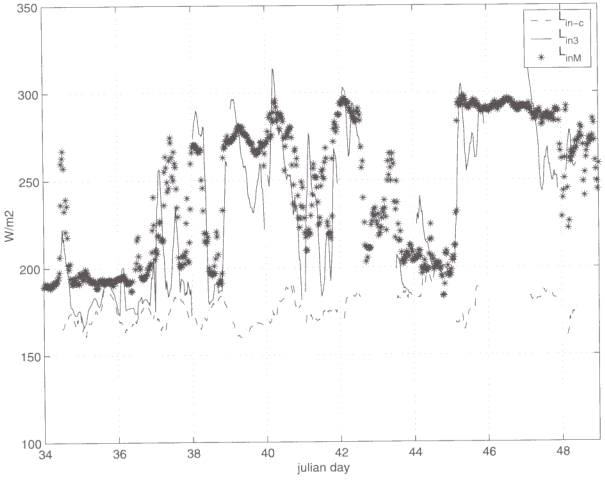

(b) Incoming longwave radiation from Swinbank [10], February 1998.

Figure 5: In the abscissa the julian days are reported. The star points refer to L_{inM}, the dashed line to L_{in-c} and the solid line to L_{in3}; all values are expressed in Wm^{-2}.

Table 3: Statistics about incoming longwave radiation fluxes

Incoming longwave radiation flux	DIFF	BIAS
L_{in1} - L_{inM} $\left(\mathrm{Wm}^{-2}\right)$	1	17
L_{in2} - L_{inM} $\left(\mathrm{Wm}^{-2}\right)$	2	17
L_{in3} - L_{inM} $\left(\mathrm{Wm}^{-2}\right)$	-4	19

water and old snow has been imposed. The results of eq. 25 smoothed using a running average of fifth order, are reported in figs. 6(a) and 6(b). In this case, the intercomparison between parameterized and measured data shows the best agreement in the second period, while in some days of the first period (particularly in the julian days 18-20) while there are some evident disagreements. They can be due to the rise of surface temperature or to the inexact value assumed for ε.

In table 4 the DIFF and BIAS values for L_{out} are shown. It can be seen how the bias has the smallest value among all parameterizations used in this study.

Table 4: Statistics about outcoming longwave radiation fluxes

Outcoming longwave radiation flux	DIFF	BIAS
L_{out} - L_{outM} $\left(\mathrm{Wm}^{-2}\right)$	4	10

3.5 Net radiation

The net shortwave radiation has been evaluated as:

$$S_{net1} = S_{in} - S_{out1} \tag{26}$$

$$S_{net2} = S_{in} - S_{out2} \tag{27}$$

In figures 7a and 7b, the intercomparisons between eqs. 26 and 27 and observed data are shown. In the whole campaign S_{net1} seems closer to the observations with respect to S_{net2}, excepting in the last few days, when it snows.

The bias for the eqs. 26 and 27 is about 20 Wm^{-2}, smaller than the bias of the single values of incoming and outcoming shortwave radiations. This value is also similar to the accuracy of the sensors.

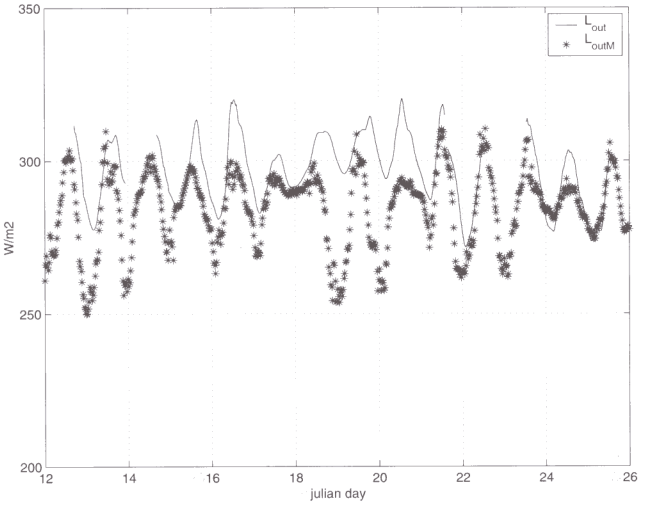

(a) Outcoming longwave radiation, January 1998.

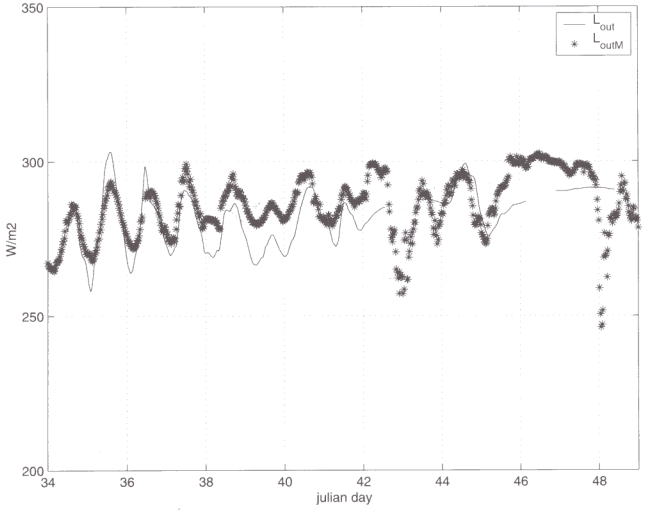

(b) Outcoming longwave radiation, February 1998.

Figure 6: In the abscissa the julian days are reported. The star points refer to L_{outM}, and the solid line to L_{out}; all values are expressed in Wm^{-2}.

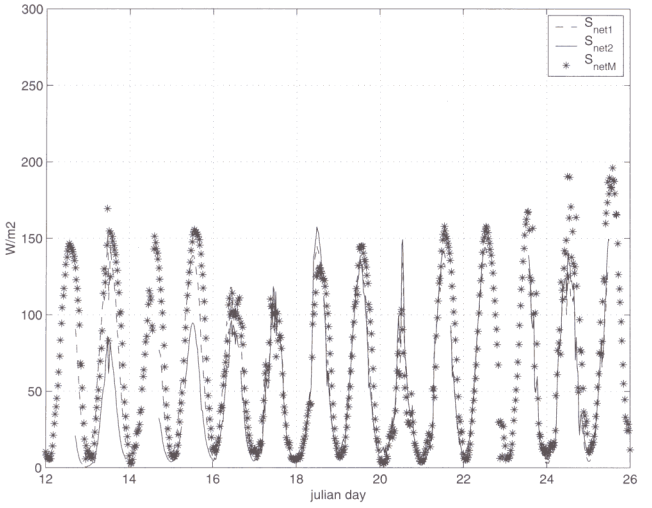

(a) Net shortwave radiation, January 1998.

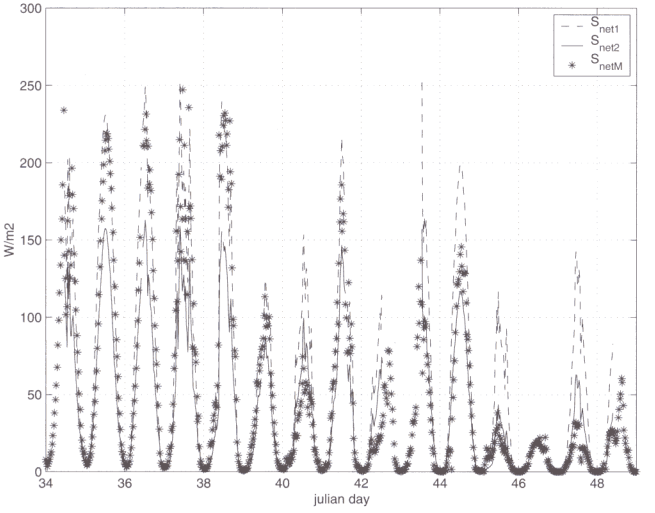

(b) Net shortwave radiation, February 1998.

Figure 7: In the abscissa the julian days are reported. The star points refer to S_{netM}, the dashed line to S_{net1} and the solid line to S_{net2}; all values are expressed in Wm^{-2}.

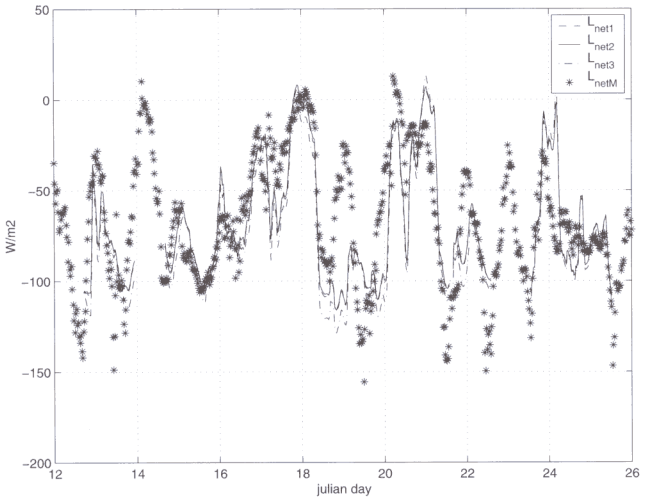

(a) Net longwave radiation, January 1998.

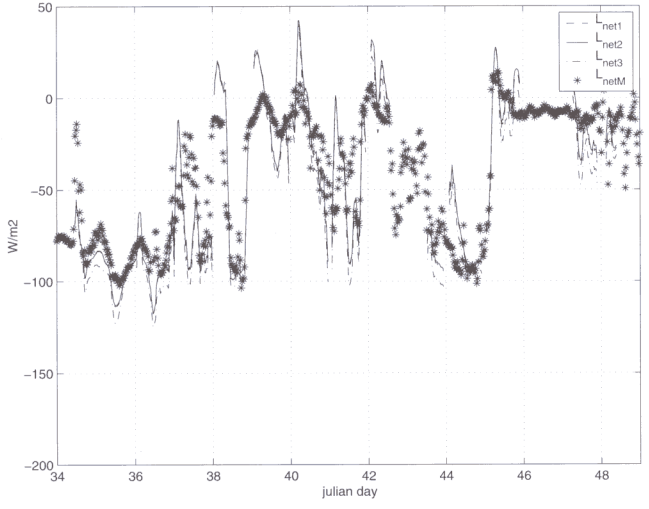

(b) Net longwave radiation, January 1998.

Figure 8: In the abscissa the julian days are reported. The star points refer to L_{netM}, dashed line to L_{net1}, the solid line to L_{net2} and the dashdot line to L_{net3}; all values are expressed in Wm^{-2}.

The net longwave radiations have been calculated as:

$$L_{net1} = L_{in1} - L_{out} \quad (28)$$
$$L_{net2} = L_{in2} - L_{out} \quad (29)$$
$$L_{net3} = L_{in3} - L_{out} \quad (30)$$

Figures 8(a) and 8(b) show the parameterizations of net longwave radiations referring to eqs. 28) - (30 respectively. Also in this case, the results were smoothed using a running average of the fifth order. The inspections of figs. 8(a), 8(b) and table 5 show that L_{net1} and L_{net2} are very similar and their accordance with the measured data is good; the bias is 20 Wm^{-2}. L_{net3} shows some differences from L_{net1} and L_{net2}, and its trend is worse than the ones of L_{net1} and L_{net2}, as evidenced by the larger bias.

Finally, the net radiation has been calculated using S_{net1} and S_{net2} for the shortwave radiation, but only L_{net1} for longwave radiation. The reason of this choice is that L_{net1} and L_{net2} are quite similar and they behave better than L_{net3}.

$$Net1 = S_{net1} + L_{net1} \quad (31)$$
$$Net2 = S_{net2} + L_{net1} \quad (32)$$

The results smoothed, using a running average of the fifth order, are represented in figs. 9(a) and 9(b). In these graphics, it is evident that Net1 is better than Net2 during the whole campaign, with the exception of the last days of February when weather conditions were snowy. This is also confirmed by the largest bias and difference (table 5).

Table 5: Statistics about net radiation fluxes

Net radiation flux		DIFF	BIAS
S_{net1} - S_{netM}	$\left(\mathrm{Wm}^{-2}\right)$	4	19
S_{net2} - S_{netM}	$\left(\mathrm{Wm}^{-2}\right)$	-14	20
L_{net1} - L_{netM}	$\left(\mathrm{Wm}^{-2}\right)$	1	20
L_{net2} - L_{netM}	$\left(\mathrm{Wm}^{-2}\right)$	2	20
L_{net3} - L_{netM}	$\left(\mathrm{Wm}^{-2}\right)$	-4	23
$Net1$ - Net_M	$\left(\mathrm{Wm}^{-2}\right)$	5.	27
$Net2$ - Net_M	$\left(\mathrm{Wm}^{-2}\right)$	-13	31

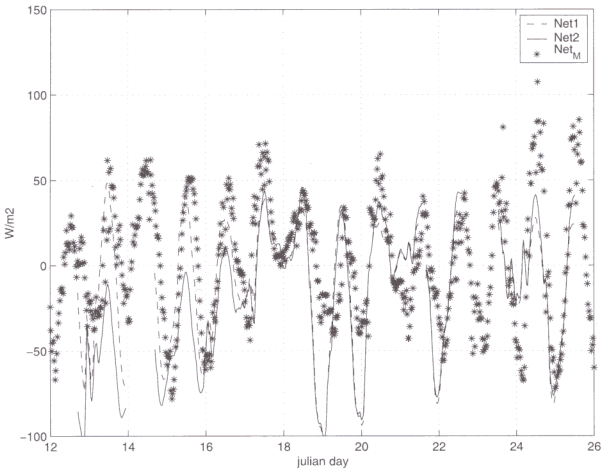

(a) Net radiation, January 1998.

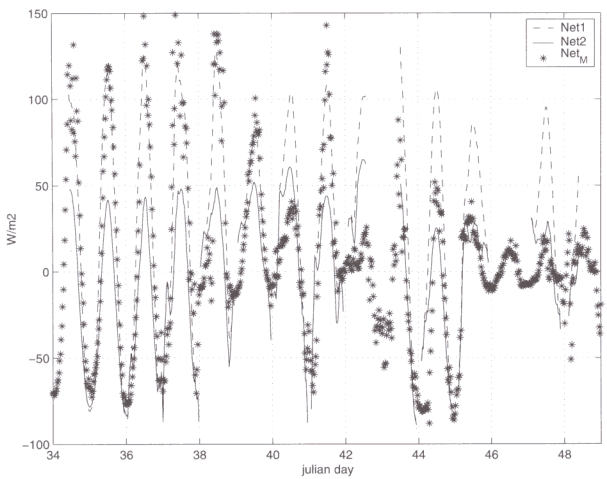

(b) Net radiation, February 1998.

Figure 9: In the abscissa the julian days are reported. The star points refer to Net_M, dashed line to Net_1 and the solid line to Net_2; all values are expressed in Wm^{-2}.

4 Conclusions and perspectives

In this work, the different components in the net radiation (incoming and outcoming shortwave and longwave) have been calculated from observa-

tions (pressure, relative humidity, surface and air temperature and incoming shortwave radiation) and compared with the measured ones. The shortwave radiation has been parameterized using 2 schemes. In both cases the parameterization is able to reconstruct the measured data with a good approximation. The longwave radiation has been parameterized using 3 different schemes. These parameterizations are more critical than the ones for the shortwave radiation, because they depend strongly on the cloudiness. In this study, cloudiness was not observed and was obtained from the real shortwave radiation and the theoretical shortwave radiation in the case of absence of cloudiness. The availability of observations of cloud coverages and cloud types could improve the parameterizations of both short and longwave components. In spite of this problems, the larger bias has been obtained in the evaluations of the shortwave radiation. Every parameterization displayed a bias value not larger than 30 Wm^{-2}. Considering that the accuracy of instruments is of the order of 15 Wm^{-2}, it can be concluded that the use of the proposed formulations (adeguately calibrated for the considered site) could allow to obtain data whose quality is only slightly lower than the one of the real observations.

References

[1] S. Ferrarese, C. Cassardo, A. Longhetto, D. Bertoni, R. Forza, G. Ficca, M. Pangia, and R. Purini, On the heat energy fluxes in the non-stationary surface boundary layer at Hells Gate, Terra Nova Bay (Antarctica), Oceanography of the Ross Sea, 1999.

[2] S. Ferrarese, D. Bertoni, C. Cassardo, G. Ficca, R. Forza, A. Longhetto, M. Pangia and R. Purini, Proceedings of the 7th Workshop of Italian Research on Antarctic Atmosphere, Bologna 22-24 October 1997, edit by M. Colacino, G. Giovannelli and L. Stefanutti, (SIF, Bologna) 1998.

[3] J. K. Page, Prediction of Solar Radiation on Inclined Surfaces edited by D. Reidel Publishing Company, 1986.

[4] N. Loglisci, C. Cassardo, G. P. Balsamo and M. W. Qian, A technical description of the Land Surface Process Model (LSMP) version 2000, Report 08/2001 Dipartimento di Fisica Generale, Università di Torino, Via P. Giuria 1 - 10125 Torino, Italy, 2001.

[5] M. Iqbal, An Introduction to Solar Radiation edited by Academic Press, 1983.

[6] B. Loth and H. F. Graf, Modeling the snow cover for climate studies, Report 190 Max-Plack Inst. fur Meteorol., Hamburg, Germany, 1996.

[7] D. L. Verseghy, *Int. J. Clim* **11** (1991) 111.

[8] D. R. Satterlund, *Water. Resour. Res.* (1979) 1649.

[9] D. O. Stanley and G. Jurica, *J. of Appl. Meteorol.* (1972) 349.

[10] W. C. Swinbank, *Quart. J. Roy. Met. Soc.* (1963) 339.

[11] J. R. Garratt, The Atmospheric Boundary Layer edited by Cambridge University Press, 1992.

[12] W. Brutsaert, Evaporation into the Atmosphere edited by D. Reidel Publishing Company, 1982.